Journal of Structural Mechanics

ISSN: 0890-5452 (Print) (Online) Journal homepage: www.tandfonline.com/journals/lmbd19

On the Design of Compliant Mechanisms Using Topology Optimization

Ole Sigmund

To cite this article: Ole Sigmund (1997) On the Design of Compliant Mechanisms Using Topology Optimization , Journal of Structural Mechanics, 25:4, 493-524, DOI: 10.1080/08905459708945415

To link to this article: https://doi.org/10.1080/08905459708945415

Published online: 02 Apr 2007.

MECH. STRUCT. & MACH., 25(4), 493–524 (1997)

On the Design of Compliant Mechanisms Using Topology Optimization*

Ole Sigmund

DEPARTMENT OF SOLID MECHANICS
TECHNICAL UNIVERSITY OF DENMARK
DK-2800 LYNGBY, DENMARK

ABSTRACT

This paper presents a method for optimal design of compliant mechanism topologies. The method is based on continuum-type topology optimization techniques and finds the optimal compliant mechanism topology within a given design domain and a given position and direction of input and output forces. By constraining the allowed displacement at the input port, it is possible to control the maximum stress level in the compliant mechanism. The ability of the design method to find a mechanism with complex output behavior is demonstrated by several examples. Some of the optimal mechanism topologies have been manufactured, both in macroscale (hand-size) made in Nylon, and in microscale (< .5mm)) made of micromachined glass.

I. INTRODUCTION

A compliant mechanism is a mechanism that gains its mobility from the flexibility of some or all of its members, as opposed to its more conventional rigid body counterpart (Fig. 1). Advantages of compliant mechanisms are that they require

*Communicated by P. Pedersen

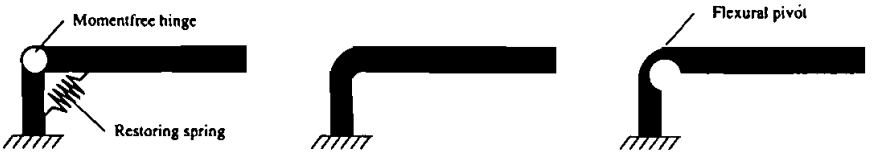

Fig. 1. A rigid body mechanism (left), a distributed compliant mechanism (center), and a lumped compliant mechanism (right).

fewer parts; are easy to fabricate; have less wear, friction, and backlash; have no need for lubrication; and have built-in restoring force [1,2]. The concept of compliant or flexible mechanisms is not new [3], but it has recently received increased attention because of the introduction of materials with superior properties and the rapidly expanding field of MicroElectroMechanical Systems (MEMS).

MicroElectroMechanical Systems are built in sub-millimeter scale and integrated with electronic circuits [4]. They are manufactured using etching techniques from the semi-conductor industry, and are already widely used for integrated sensor applications; e.g., acceleration sensors for airbags. They have potential applications for in-body surgery, health monitoring, micromanipulation, and nano-fabrication [5]. Compliant mechanisms are well-suited for MEMS because of the small length scale and problems with friction and wear that prohibit use of conventional rigid-body mechanisms.

Because of the complexity of elastic behavior of compliant mechanisms, their design has typically been accomplished by trial and error methods. However, researchers have addressed the question of introducing more systematic design procedures. Non-linear finite element analysis and optimization methods have been used to design flexible mechanisms for function generation [1]. Studies [6,7,8,9] began by synthesizing a rigid-body mechanism, in turn introducing flexibility to obtain a pseudo-rigid-body mechanism, and finally analyzing a fully compliant mechanism. These design methods include the so-called shooting methods or chain-methods. The synthesis problem has been considered in many other works. Common to all methods, however, is that they consider the dimensional design or modification of a fixed mechanism topology, typically a four-bar mechanism. An interesting approach to the design of compliant mechanisms, which allows for change of topology, is to make use of *topology optimization methods* [10,11]. Topology optimization methods were originally intended for maximum stiffness design of elastic structures, but has recently been extended to the design of compliant mechanisms by Anathasuresh et al. [12], who demonstrated the design of a simple crunching mechanism; Sigmund [13], who designed gripping mechanisms using a truss topology model; and Larsen et al. [14], who designed topologically complicated mechanisms with multiple input and output ports using a continuum-type topology optimization method.

In this paper, the concept and methods of using continuum-type topology optimization for the design of compliant mechanisms if presented. It is demonstrated that the maximum stress in a compliant mechanism can be controlled by introducing a displacement constraint at the input port. It is shown that the optimal compliant mechanism topology is highly dependent on the work task considered. In the literature, compliant mechanisms have been categorized as distributed or lumped compliant mechanisms, as sketched in Fig. 1. Subject to an input load, fully compliant mechanisms bend throughout the structure, whereas lumped compliant mechanisms bend in flexural hinges. This paper shows that both distributed and lumped compliant mechanisms can be optimal, depending on the work-task considered. Finally, some of the mechanisms obtained by the design procedure are built and tested, both in macroscale (made of Nylon) and in microscale (made of glass).

The paper has seven main sections; Section 1 is the introduction, Section 2 discusses the design problem, Section 3 discusses the finite element analysis necessary to determine performance of compliant mechanisms, Section 4 discusses how the topology optimization problem is solved using sequential linear programming, Section 5 shows several examples of compliant mechanism design using the proposed procedure, Section 6 descries how some of the compliant mechanisms were manufactured in microscale using lasermicromaching techniques and tested using external probes, and Section 7 presents conclusions. Appendix 1 contains the sensitivity analysis, and Appendix 2 briefly describes a procedure to obtain mesh-independency of the solutions.

II. THE DESIGN PROBLEM

A compliant crimping mechanism is shown in Fig. 2. The mechanism is assumed to lie within the domain Ω. When the mechanism is subjected to a force F_{in} at the input port, it will deflect, resulting in a force F_{out} on the workpiece.

The optimal design of a complaint mechanism depends on factors such as the manipulation task it should perform, the material of which it is made, and the available input force or actuator. It also depends on the available design space. Possible manipulation tasks can be crunching or clamping or workpieces, path generation, prescribed input/output force/deflection relationships, desired energy storage, and many others. This section concentrates on crunching mechanisms and mechanisms with smaller displacements. This allows use of linear (small) displacement finite element analysis, which is computationally simple. However, most of the derivations and ideas in this paper can be extended on non-linear displacement theory, in turn allowing synthesis of path generating and other large displacement mechanisms.

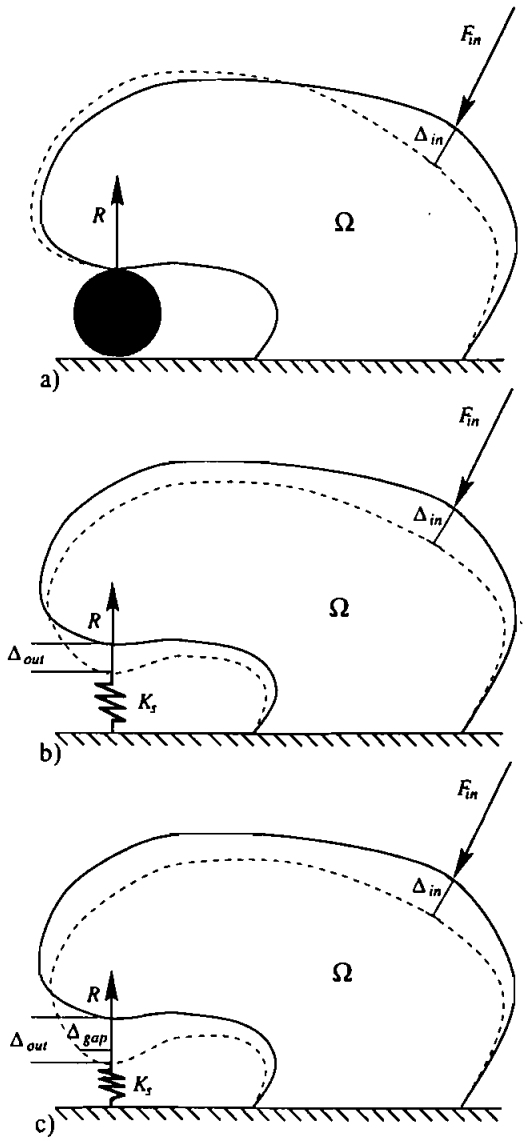

Fig. 2. Three different situations: (a) stiff workpiece and zero gap ($\Delta_{gap} = 0$); (b) elastic workpiece and zero gap; and (c) elastic workpiece and gap between workpiece and output port ($\Delta_{gap} > 0$).

The major design goal for crunching mechanisms is maximization of the output force F_{out} (the force on the workpiece) for a given input force F_{in}. *The ratio between the output and input forces $M = F_{out}/F_{in}$ is called the Mechanical Advantage.* The mechanical advantage is dependent on the size and stiffness K_s of the workpiece [15]. Figure 2 shows three different situations;

(1) When the workpiece is stiff and fills the gap under the output port; i.e., $\Delta_{gap} = \Delta_{out} = 0$, the input force can be transferred directly to the workpiece (Fig. 2a).
(2) When the workpiece is elastic, but fills out the gap under the output port (i.e., $\Delta_{gap} = 0$), the output port must move (i.e., $\Delta_{out} > 0$) before the workpiece will be stressed (Fig. 2b). This means that some of the work done by the input force is used to deflect the mechanism. If there is no workpiece, or if it is very soft, all or most of the input work is stored as internal energy in the mechanism.
(3) If there is a gap between the output port and the workpiece; i.e., $\Delta_{gap} > 0$, some of the input work is stored as internal energy in the mechanism before contact (Fig. 2c). If the mechanism is too stiff, or if the input force is too small, only low (if any) values of the mechanical advantage can be obtained.

As ca be seen, there are conflicting objectives. On one hand, the mechanism should be stiff to be able to transmit a high force to the workpiece. On the other hand, it should be soft enough to deflect and make contact with the workpiece.

Three constraints are important in the synthesis of compliant mechanisms: (1) a constraint on the maximum stress in the mechanism (to hinder fatigue or failure), (2) a constraint on deflection at the input port, and (3) a constraint on volume to save material and cost and to allow underetching in the processing of MEMS. Since stress constraints in continuum-type topology optimization is difficult and has not been addressed in the literature so far, stress constraints will not be considered here. *Nevertheless, the maximum stress levels in compliant mechanisms can be controlled indirectly by constraining displacement at the input port.* This will be demonstrated in the example section.

The design problem can be defined as the problem of finding the optimal mechanism topology within a design domain Ω that satisfies the above-mentioned goals and constraints. *The optimal compliant mechanism may be found, in an optimal way by distributing a limited amount of material in the design domain.* This optimization problem is a "topology optimization problem," and it can be solved using techniques from the field of topology optimization, as will be shown in this paper.

An optimization formulation of the above-mentioned problem can be written as follows:

Maximize : Mechanical Advantage M

$$\begin{aligned} \textit{Subject to}: &\quad \text{Volume constraint } V \le V^* \\ \textit{and}: &\quad \text{Input displacement } \Delta_{\text{in}} \le \Delta_{\text{in}}^* \end{aligned} \tag{1}$$

where V^* and Δ_{in}^* are allowed volume and input displacement, respectively.

The mechanical advantage and input displacement are functions of the size and stiffness of the workpiece, as well as of the material distribution. In the next section, it is shown that M and Δ_{in}, for numerous kinds of workpieces can be calculated by solving a finite-element problem with only two load cases.

III. MECHANICAL ANALYSIS

This section shows how the mechanical advantage and displacement at the input port of a compliant mechanism can be found by discretizing the compliant mechanism using finite elements and solving equilibrium equations for two load cases.

Assuming that the design domain Ω has been discretized using N finite elements, two load cases shown in Fig. 3 are defined. The first load case consists of the input load $p_1 = F_{\text{in}}$, defined by the finite element load vector $\mathbf{F}_1$. The second load case is a unit dummy load p_2 at the output port, defined by the finite element load vector $\mathbf{F}_2$. The dimension of both $\mathbf{F}_1$ and $\mathbf{F}_2$ is two times the number of nodes, which is equal to the number of degrees of freedom in the finite element model.

Using the dummy load method, displacements Δ_{ij} can be found, where indices ij indicate displacement at port i, due to a load at port j. Displacements Δ_{ij} are used to calculate the mechanical advantage and input deflection. They can be written in the bilinear forms

$$\begin{aligned} \Delta_{11} &= \mathbf{D}_1^T \mathbf{S} \mathbf{D}_1 / p_1, & \Delta_{12} &= \mathbf{D}_2^T \mathbf{S} \mathbf{D}_1 / p_1 \\ \Delta_{22} &= \mathbf{D}_2^T \mathbf{S} \mathbf{D}_2 / p_2, & \Delta_{21} &= \mathbf{D}_1^T \mathbf{S} \mathbf{D}_2 / p_2 \end{aligned} \tag{2}$$

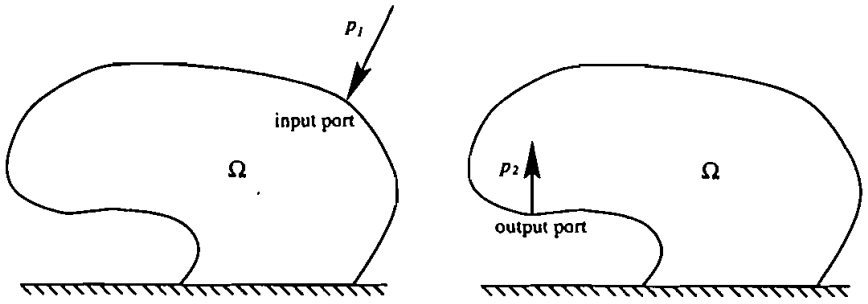

Fig. 3. Two load cases. Input force (left) and output dummy load (right).

where $\mathbf{S}$ is the global finite element stiffness matrix, and $\mathbf{D}_1$ and $\mathbf{D}_2$ are nodal displacement vectors that are found as solutions of the finite element problems

$$\mathbf{SD}_1 = \mathbf{F}_1, \quad \mathbf{SD}_2 = \mathbf{F}_2 \tag{3}$$

Note that Δ_{11} and Δ_{21} correspond to displacements at the input and output ports, respectively, if there is no resistance for a workpiece. Although p_1 is a unit load, it is nevertheless kept in Eq. 2 to give the proper dimension (meters).

In the next three subsections, the mechanical advantage and input displacement are calculated as functions of Δ_{ij}, for the three cases of workpieces shown in Fig. 2.

A. No gap, stiff workpiece

As defined earlier, the mechanical advantage M is the ratio of reaction (output) force at the output port R and input force; i.e., $M = F_{\text{out}}/F_{\text{in}} = R/p_1$. For the case of a stiff workpiece and no gap between the output port and the workpiece (Fig. 2a), the reaction force is calculated as the force at the output port that gives zero displacement at the output port when the workpiece is removed. In practice, the reaction force is calculated as $R = cp_2$, where c is the factor with which the displacement Δ_{22} due to the unit dummy load p_2 applied at the output port must be multiplied, to give zero displacement at the output port; i.e.,

$$\Delta_{21} - c\Delta_{22} = 0, \quad c = \frac{\Delta_{21}}{\Delta_{22}} \tag{4}$$

The reaction force at the output port is then found as

$$R = cp_2 = \frac{\Delta_{21}}{\Delta_{22}} p_2 \tag{5}$$

Thus, the mechanical advantage can be written as

$$M = R/p_1 = cp_2/p_1 = \frac{p_2}{p_1}\frac{\Delta_{21}}{\Delta_{22}} \tag{6}$$

Displacement at the input port Δ_{in} is defined as displacement in the direction of the input force. It can be found by solving the combined load case consisting of p_1 and R. However, since consideration is limited to linear elasticity, the resulting displacement vector $\mathbf{D}_R$ for the combined load case is a superposition of the displacement vectors $\mathbf{D}_1$ and $\mathbf{D}_2$. That is,

$$\mathbf{D}_R = \mathbf{D}_1 - c\mathbf{D}_2 \tag{7}$$

or,

$$\Delta_{\text{in}} = \Delta_{11} - c\Delta_{12} \tag{8}$$

B. No gap, elastic workpiece

For the case of no gap and an elastic workpiece, the stiffness of the workpiece is defined as K_s, and the displacement of the spring is $\Delta_{spring} = \Delta_{out}$. The spring force equilibrates the reaction force; i.e.,

$$R = \Delta_{spring} K_s = \Delta_{out} K_s, \quad \Delta_{out} = \frac{R}{K_s} \tag{9}$$

For this case, c is the factor by which the displacement Δ_{22} must be multiplied to give the displacement Δ_{out} at the output port; i.e.,

$$\Delta_{21} - c\Delta_{22} = \Delta_{out} \tag{10}$$

or, solving for c,

$$c = \frac{\Delta_{21} - \Delta_{out}}{\Delta_{22}} = \frac{\Delta_{21} - R/K_s}{\Delta_{22}} \tag{11}$$

Substituting c into $R = cp_2$ and solving for the reaction force gives

$$R = p_2 \frac{\Delta_{21}}{\Delta_{22} + p_2/K_2} \tag{12}$$

Thereby, the mechanical advantage can be written as

$$M = R/F_{in} = R/p_1 = \frac{p_2}{p_1} \frac{\Delta_{21}}{\Delta_{22} + p_2/K_2} \tag{13}$$

The input displacement is found, as before, using Eq. 8 and c from Eq. 11.

It can be seen that, for K_s approaching infinity, the mechanical advantage of Eq. 13 approaches the mechanical advantage for a stiff workpiece in Eq. 6.

C. Gap, elastic workpiece

For the case $\Delta_{gap} > 0$ and an elastic workpiece, the displacement of the spring (workpiece) is $\Delta_{spring} = \Delta_{out} - \Delta_{gap}$. The spring force equilibrates the reaction force, thus

$$R = \Delta_{spring} K_s = (\Delta_{out} - \Delta_{gap}) K_s, \quad \Delta_{out} = \frac{R}{K_s} + \Delta_{gap} \tag{14}$$

where it is assumed that the gap is closed; i.e., $\Delta_{out} \geq \Delta_{gap}$. For this case, c is the factor by which the displacement Δ_{22} must be multiplied, to give the displacement Δ_{out} at the output port; i.e.,

$$\Delta_{21} - c\Delta_{22} = \Delta_{out} \tag{15}$$

or, solving for c,

$$c = \frac{\Delta_{21} - \Delta_{out}}{\Delta_{22}} = \frac{\Delta_{21} - R/K_s - \Delta_{gap}}{\Delta_{22}} \tag{16}$$

Substituting c into $R = cp_2$ and solving for the reaction force gives

$$R = p_2 \frac{\Delta_{21} - \Delta_{gap}}{\Delta_{22} + p_2/K_s} \tag{17}$$

Thereby, the mechanical advantage can be written as

$$M = R/F_{in} = R/p_1 = \frac{p_2}{p_1} \frac{\Delta_{21} - \Delta_{gap}}{\Delta_{22} + p_2/K_s} \tag{18}$$

Input and output displacements are found, as in Eq. 8, but with c defined by Eq. 16.

It can be seen that for $\Delta_{gap} = 0$ and $K_s =$ infinity, the mechanical advantage of Eq. 18 is equal to the mechanical advantage for zero gap and a rigid workpiece in Eq. 6. Similar observations hold for input and output displacements Δ_{in} and Δ_{out}. This means that all combinations of workpiece stiffness and gaps are contained in Eqs. 18, 16, 10, and 8, and they can be found only by solving two finite element load cases defined in Eq. 3.

D. Design discretization and material model

Following standard topology optimization methods, the design domain for a compliant mechanism is discretized by N bilinear finite elements. Space restrictions may limit the area that the optimal compliant mechanism is allowed to occupy. For computational simplicity, a simple rectangular design domain and a regular finite element mesh are selected. In practice, however, any shape of the design domain can be used.

Allowing each finite element in the design domain to be either solid or void, it is possible to describe the topology of a compliant mechanism by "turning on or off" each pixel-like finite element. With a fine discretization (using several thousand finite elements), detailed compliant mechanism topologies can be modeled, as will be demonstrated in the examples section.

This is an integer design problem, and an intuitive approach to solve the optimization problem could be to try out all possible mechanism topologies defined by all possible combinations of finite element pixel patterns; evaluate the cost functions and constraints for each topology; and pick the topology that has the lowest value of the cost function and satisfies the constraints. However, the number of possible topologies is astronomical, even for a small number of elements (i.e., $2^{100} = 1.27 \cdot 10^{30}$ topologies, for $N = 100$). Hence, the combinatorial problem is impossible to solve. Following the idea of standard topology optimization procedures, the problem is relaxed by allowing the material "density" in each element to take intermediate values denoted $x^e \in [x_{\min}, 1]$. This relaxation makes it possible to find continuous sensitivities of the objective functions with respect to changes in design variables x^e in turn allowing the use of mathematical programming methods to solve the optimization problem. At the end of the optimization procedure, however, the design variables should take the extreme values $x_{\min}$ or 1. For computational reasons (singularity of the finite element stiffness matrix), the values of the design variables are not allowed to be zero, but are constrained to be greater or equal to $x_{\min}$. Choosing $x_{\min}$ small (e.g., $x_{\min} = 10^{-3}$), elements with $x^3 = x_{\min}$ have no structural significeance.

For the purpose of modeling the material properties in elements with intermediate values of the element density variable x^e, the following material model is used to relate Young's modulus E^e in element e to the value of the density x^e in element e:

$$E^e = (x^e)^\eta E^0, \quad e = 1, \ldots, N \tag{19}$$

where E^0 is Young's modulus of solid material, and $\eta > 1$ is a penalization factor that is used to enforce extreme values of the design variables. By specifying a value of η greater than one, the stiffness of elements with intermediate densities is lowered, thus making it "uneconomical" to have intermediate densities in the optimal design. Based on experience, $\eta = 3$ is chosen.

IV. OPTIMIZATION ALGORITHM

To allow for underetching in the processing of micromechanisms, the maximum size or width of parts in the optimal topology is restricted. So far, no method exists within the topology optimization method to control such maximum local length scales. However, simply constraining the amount of material that can be distributed in the design domain makes it possible to indirectly control the maximum local length scales.

The total volume of material V in the design domain can be found as a sum over the N finite elements used to discretize the design domain,

$$V = \mathbf{v}^T \mathbf{x} \tag{20}$$

where $\mathbf{x}$ and $\mathbf{v}$ are N-vectors containing the element densities (design variables) and element volumes, respectively.

Now, the mechanical advantage, input displacements, and total volume of a compliant mechanism design have been defined, as functions of the vector $\mathbf{x}$ of element densities, or design variables. The discretized version of the optimization problem of Eq. 1 can thereby be written as

$$\begin{aligned} \textit{Minimize}: \quad & -M(\mathbf{x}) \\ \textit{Subject to}: \quad & \Delta_{\text{in}}(\mathbf{x}) \leq \Delta_{\text{in}}^* \\ : \quad & V(\mathbf{x}) = \mathbf{v}^T \mathbf{x} \leq V^* \\ : \quad & \mathbf{S}(\mathbf{x})\mathbf{D}_1(\mathbf{x}) = \mathbf{F}_1, \quad \mathbf{S}(\mathbf{x})\mathbf{D}_2(\mathbf{x}) = \mathbf{F}_2 \\ : \quad & \mathbf{0} < \mathbf{x}_{\min} \leq \mathbf{x} \leq \mathbf{1} \end{aligned} \tag{21}$$

where boldface symbols indicate N-vectors and the maximization problem has been converted to a minimization problem by multiplying the objective function by -1.

A. Sequential Linear Programming

Topology optimization problems are often solved using optimality criteria methods. These methods are very efficient for solving optimization problems with simple objective functions (compliance), one constraint (on volume), and many variables. However, the methods are generally based on heuristic updating schemes. They are difficult to generalize to more complicated cost functions and multiple constraints, and final convergence is often slow. Therefore, a mathematical programming method called Sequential Linear Programming (SLP) is used to solve the optimization problem in this work. The SLP method consists of sequentially solving an approximate linear subproblem that is obtained by writing linear Taylor series expansions for the objective and constraint functions. The SLP method has been used successfully in many types of standard structural optimization problems [16]. It has been evaluated as robust and efficient [17], and has been used in topology optimization of material composites with extreme thermal expansion [18].

The SLP method solves the optimization problem of Eqs. 21 iteratively. For each iteration step, a finite element analysis is performed, and the optimization problem is linearized around the current design point $\mathbf{x}$, using the linear part of

Taylor series expansions; i.e.,

$$\begin{aligned} \textit{Minimize}: \quad & -M - \left\{\frac{\partial M}{\partial \mathbf{x}}\right\}^T \Delta\mathbf{x} \\ \textit{Subject to}: \quad & \left\{\frac{\partial \Delta_{\text{in}}}{\partial \mathbf{x}}\right\}^T \Delta\mathbf{x} \le \Delta_{\text{in}}^* - \Delta_{\text{in}} \\ : \quad & \left\{\frac{\partial V}{\partial \mathbf{x}}\right\}^T \Delta\mathbf{x} = \mathbf{v}^T \Delta\mathbf{x} \le V^* - V \\ : \quad & \Delta\mathbf{x}_L \le \Delta\mathbf{x} \le \Delta\mathbf{x}_U \end{aligned} \tag{22}$$

where $\Delta\mathbf{x}_L$ and $\Delta\mathbf{x}_U$ are N-vectors containing move-limits on the design variables, and $\Delta\mathbf{x}$ is the N-vector of design changes. The move-limits are adjusted for absolute limits given in Eq. 21.

The optimization problem of Eq. 22 is a linear programming problem, and the optimal change in design $\Delta\mathbf{x}$ is found using the Simplex method (here, the linear programming solver DSPLP [19] from the SLATEC library is used). The move-limit strategy is important for stable convergence of the SLP algorithm. Here, the move-limit for a specific design variable is increased by a factor of 1.3 if the change of the design variable has the same sign in two successive steps. Similarly, the move-limit is decreased by a factor of 0.6 if the change in the design variable has opposite signs for two successive steps.

Solving the linear programming problem of Eq. 22 requires the determination of sensitivities of the mechanical advantage and input displacement to a change in design variable ($\partial M/\partial x^e$ and $\partial \Delta_{\text{in}}/\partial x^e$, respectively). The sensitivity analysis is derived in Appendix 1 and can be computed based on the two finite element load cases already solved.

A flowchart of the design algorithm is shown in Fig. 4. Describing the individual steps briefly, the finite element problem is first initialized and regions in the design domain that are fixed to be either solid or void are defined. The material in the remaining elements is evenly distributed so that the volume constraint is satisfied. After initialization, the sequential process of alternating finite element analysis, sensitivity analysis, LP-solving, and updating the design variables is followed. When the change in design variables in two successive iterations is less than 10^{-4} (by experience), the procedure is declared to have converged, and the resulting topology is plotted.

Compared to typical topology optimization problems for minimum compliance, the present design problem requires many more iterations to converge (several hundred, compared to perhaps 50 iterations). This can be explained by the fact that the present objective and constraint functions are non-self-adjoint and, therefore, more complex than usual compliance optimization problems. Experience also

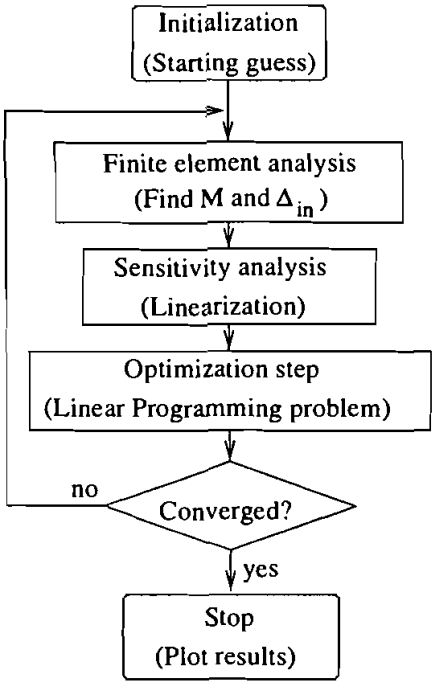

Fig. 4. Flowchart of the design algorithm.

shows that the SLP method occasionally has a tendency to violate constraints. Better convergence properties might be obtainable if the SLP method is substituted with a dual method and convex approximation of objective and constraint functions. The test of other optimization algorithms will be the subject of future research.

B. Problems related to topology optimization

This subsection discusses numerical difficulties due to the finite-element discretization; namely, checkerboard patterns, mesh-dependencies, and local minima.

1. Checkerboard and mesh-dependency problems. Applying the topology optimization method to different design problems, one often encounters regions of alternating solid and void elements, referred to as checkerboards in the "optimal solution." The regions are seen in many works on topology optimization, and it was earlier believed that such regions represented optimal microstructure at the finite element level. However, two recent papers [20,21] conclude that regions with checkerboard patterns have artificially high (numerical) stiffness (higher than

the theoretical bounds) and can be explained by poor numerical modeling of the stiffness of checkerboards by low order finite elements. Both papers conclude that checkerboards are prone to appear in topology optimization using four-node linear displacement finite elements, as here, but also in topology optimization using higher order elements such as nine-node quadratic displacement finite elements.

Another problem, due to finite-element discretization, is mesh-dependency or non-existence of solutions, which refers to nonconvergence of solutions with mesh refinement. Refining the finite element mesh ideally should result in the same topology as a coarse mesh, but with better definitions of the boundaries between the material phases. However, a refinement does result in a solution with a more complicated (finer) microstructure. The problem of non-existence of solutions can be avoided by imposing extra restrictions on the design problem, as has been suggested in recent papers. Two papers have presented mesh-independency methods that are theoretically well founded and have proofs of existence of solutions. The first paper [22] suggests introducing a constraint on global perimeter. The second paper [23] introduces a slope constraint on the variation of densities from element to element. Two heuristic (but computationally much simpler) approaches have also been suggested. A paper on bone remodelling [24], closely related to topology optimization methods, suggests a mesh-independency algorithm that assumes that bone growth at a point is dependent on loads in a (mesh-independent) neighborhood of the point. A method related to this approach, but with different origin [25], performs the density update based on low-pass filtered strain energy fields. The latter approach produces optimal designs that are almost identical to the designs described by Petersson and Sigmund [23]. Due to its computational simplicity and efficiency, the heuristic approach suggested by Sigmund [25] will be used to avoid the checkerboard and mesh-dependency problems. Since the thesis by Sigmund [25] is not generally available, the mesh-independency algorithm is briefly described in Appendix 2.

2. Local minima. Topology optimization methods are prone to converge to local minima. However, introducing the mesh-independency algorithm (Appendix 2) makes it possible to prevent this problem, to a certain extent. Solving a design problem is then typically done as follows. First, the optimization problem is solved with a low value of the low-pass filter parameter; i.e., rapid variation in element densities is not allowed. This results in a design with large areas of intermediate densities, but it also prevents the design from converging to a local minimum (binary design). Gradually, the low-pass filter parameter is increased, in turn enabling the design problem to converge. In this way, a solution is generally produced that has few intermediate density elements and that is, by experience, a near-global optimum. The same procedure was used for the design of material structures with extreme thermoelastic properties by Sigmund and Torquato [18] and gave results close to theoretical bounds.

V. EXAMPLES

To demonstrate the design procedure, this section presents several examples. Subsections A and B consider the design of macroscopic (hand-size) tools made of Nylon, whereas subsections C and D consider the design of microscopic mechanisms made of glass. In subsection A, the influence of constraining the input displacement and the influence of workpiece stiffness and size on the optimal mechanism topology is demonstrated. In subsection B, the optimal topology's dependence on the design space is demonstrated. Subsection C shows how the design method can be extended to include multiple output ports, and subsection D, the design of a displacement inverter and amplifier is demonstrated.

A. Crunching mechanism

To demonstrate the effect of constraining input displacement and the effect of size and stiffness of the workpiece, the design problem sketched in Fig. 5 is considered. The design domain is a rectangular region. White and black areas denote regions that are fixed to be void or solid, respectively. The mechanism is supported at the left side and is subject to a vertical input load F_{in} at the upper and lower right corners. The objective function is to maximize the force on the workpiece (grey circle) under the piston, by distributing material in the grey area (design area). Using symmetry, the upper half of the structure is discretized using $N = 120 \cdot 40 = 4800$ finite elements. The base material for the mechanism is Nylon, which has Young's modulus $E = 3GPa = 3000N/(\text{mm})^2$, Poisson's

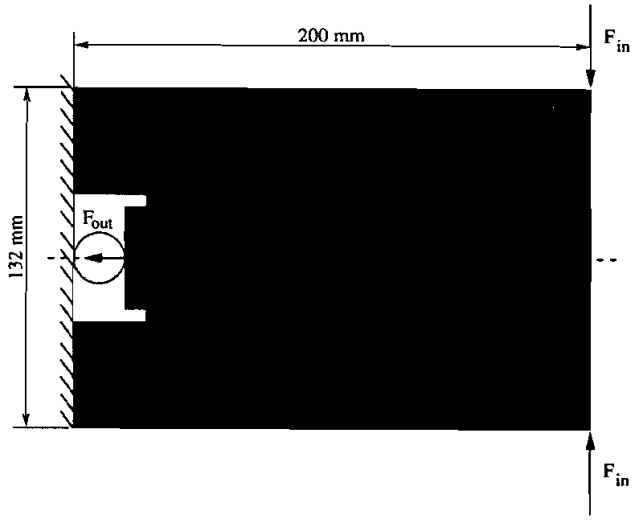

Fig. 5. Design domain for the crunching mechanism.

ratio $\nu = 0.4$, and yield strength $\sigma_f = 0.1GPa = 100N/(\text{mm})^2$. The thickness is $t = 10\,\text{mm}$, the allowable amount of material is 33%, and the input load is $F_{in} = 50N$.

First, the design problem is solved for $\Delta_{gap} = 0$, a stiff workpiece, and varying values of the allowable displacement Δ_{in}^* at the input port. The resulting topologies for $\Delta_{in}^* = 0.2$, 0.5, 1.0, 2.0, and 5.0 mm are shown in Figs. 6a–6e, respectively. Data for the five examples are shown in Table 1. Studying the optimal topologies in Fig. 6, it can be seen that they change significantly with the allowed value of Δ_{in}^*. For a small value of input displacement (Fig. 6a), the mechanism must be very stiff, and the resulting mechanical advantage is low ($M = 0.99$), as seen in

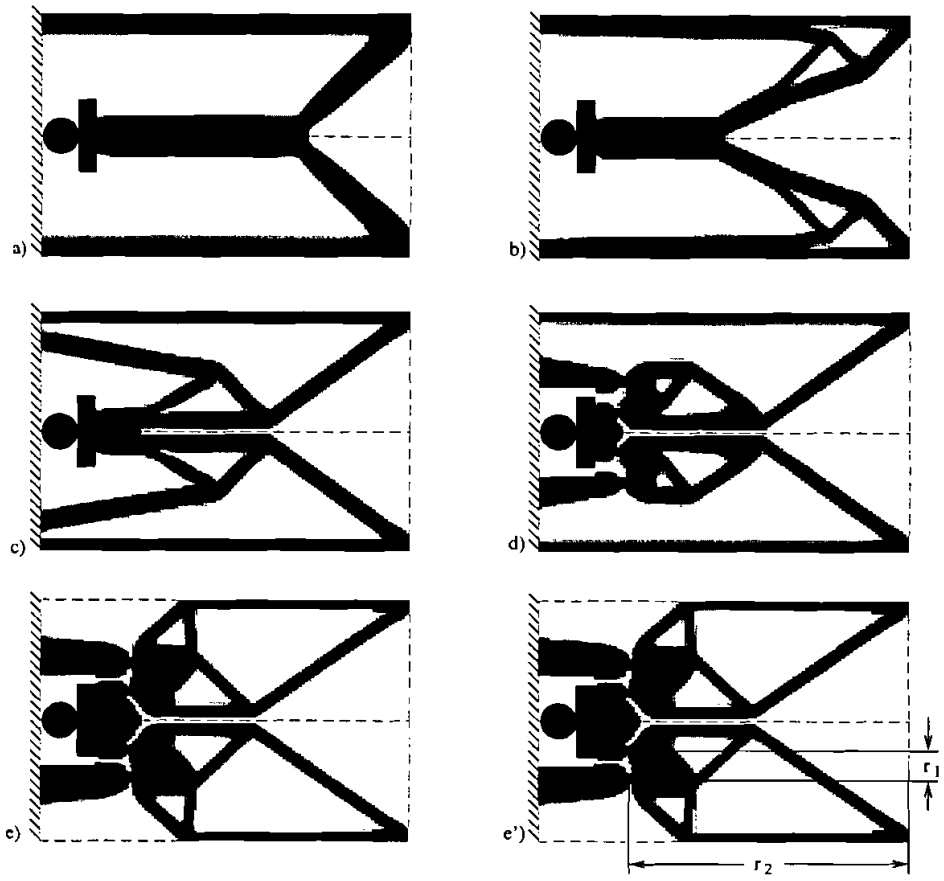

Fig. 6. Optimal crunching mechanism topologies for zero gap and varying input displacement: (a) $\Delta_{in} = 0.1$; (b) $\Delta_{in} = 0.25$; (c) $\Delta_{in} = 0.5$; (d) $\Delta_{in} = 1.0$; (e) $\Delta_{in} = 2.5\,\text{mm}$.

TABLE 1
Data for crunching mechanisms with zero gap.

Example	Δ_{in}^{*} mm	σ_{max} $N/(mm)^2$	M
a	0.10	13	0.99
b	0.25	19	1.84
c	0.50	27	3.17
d	1.00	108	5.30
e	2.50	172	8.50

Table 1. When a higher value of the input displacement is allowed (e.g. Fig. 6e), the mechanism can be softer, which in turn allows a higher value of mechanical advantage ($M = 8.5$). A rough estimate of the value of mechanical advantage of mechanism *e* can also be obtained as the ratio between the lever lengths r_1 and r_2 found from Fig. 6d; i.e., $M_{est.} = r_2/r_1 = 44\,\text{mm}/5\,\text{mm} = 8.8$. One could conclude that the optimal mechanical advantage is obtained by allowing large input displacements. However, studying Table 1 shows that the maximum von Mises stress σ_{max} in the mechanisms increases with allowable input displacement. This can also be explained by studying Fig. 6. In example *a*, the input force is transferred to the output port through wide structural elements, whereas the input force is transferred through narrow hinge-like elements in example *e*, resulting in the low stress of example *a* and the high stress of example *e*. *This example indicates that the maximum stress level can be controlled indirectly by constraining the input displacement.* When the maximum von Mises stress exceeds $100N/(mm)^2$ (yield stress of Nylon), the mechanisms will break for the given input load. Allowing a safety factor of 1.5, the stress limit is $66N/(mm)^2$, which means that the optimal crunching topology for the given input load would be a topology somewhere between examples *c* and *d*.

Next, the design problem is solved for varying values of the gap between the output port and the workpiece ($\Delta_{gap} = 0.5$, 1.0, and 6.0 mm) and stiff workpiece. The resulting topologies are shown in Figs. 7f–7h, respectively. The input displacement was constrained to the input displacement of mechanism *b*, for the given gaps. Data of the three examples are shown in Table 2. The first two rows of Table 2 show that the maximum stress in mechanism *b* increases if $\Delta_{gap} > 0$ (for which is was not designed). Therefore, the mechanisms must be designed for the specific work task. As discussed in section 2, the optimal mechanism must be soft enough to close the gap between the output port and the workpiece, and at the same time stiff enough to transmit the input force to the workpiece after contact. This is reflected in the optimal topologies. For $\Delta_{gap} = 0.5$ mm (Fig. 7f), the optima topology resembles that of example *b*, but a hinge-like narrow region has appeared to allow for the larger displacement, without increasing the stress. By increasing

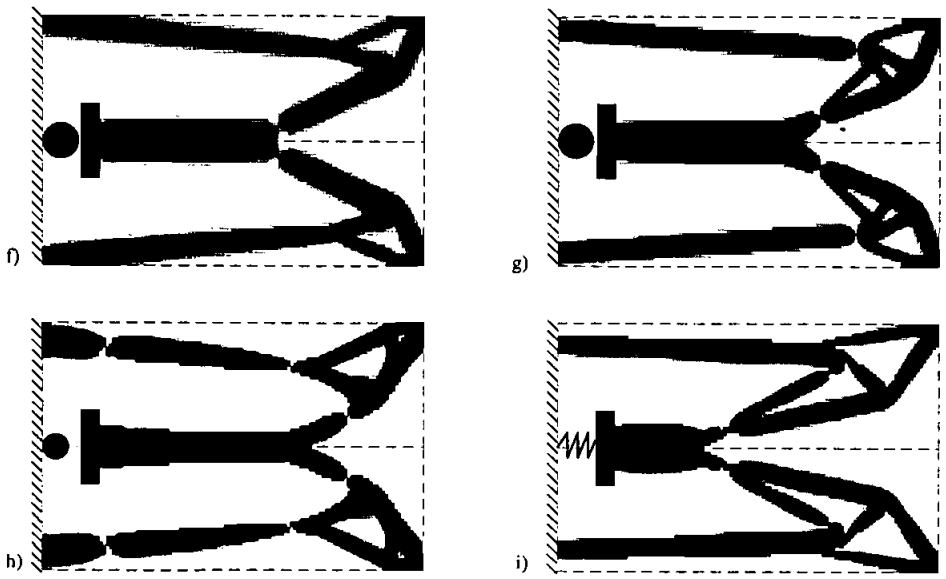

Fig. 7. Optimal crunching mechanism topologies for varying gap and input displacement: (f) $\Delta_{in} = 1.1$, $\Delta_{gap} = 0.5$; (g) $\Delta_{in} = 2.0$, $\Delta_{gap} = 1.0$; (h) $\Delta_{in} = 10.9$, $\Delta_{gap} = 6$; and (i) $\Delta_{in} = 1.5$ mm and elastic workpiece (cork).

TABLE 2
Data of crunching mechanisms with gap.

Example	Δ_{in}^* mm	Δ_{gap} mm	Δ_{out} mm	σ_{max} $N/(mm)^2$	M
b	—	0.5	0.5	53	1.53
b	—	1.0	(1.0)	86	(1.22)
f	1.1	0.5	0.5	63	1.61
g	2.0	1.0	1.0	53	1.63
h	10.9	6.0	6.0	60	1.72
i (cork)	1.5	—	0.41	81	2.46

Δ_{gap} further (Figs. 7g and 7h), hinges are formed to allow for the even larger displacements. It should be noted here that the "hinges" cannot be modeled correctly by the finite element discretization employed. *The actual design for the optimal shapes for the hinges must be considered separately.* This design problem will be addressed in future research. Nevertheless, the proposed design method suggests the optimal placement and number of hinges and the finite element analysis gives the designer an estimate of the maximum stress level in the compliant mechanism.

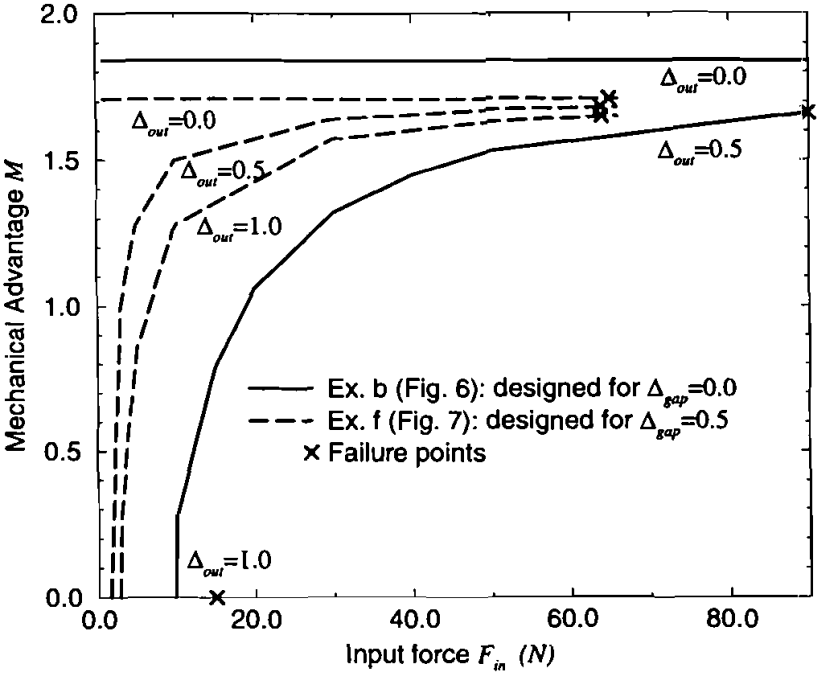

Fig. 8. Mechanical advantage to input force relationship for compliant crunching mechanism.

To further explain the behavior of the compliant mechanisms from examples *b* and *f*, their mechanical advantage to input force relationship is plotted in Fig. 8. The solid lines indicate the behavior of example *b*. For zero gap, mechanism *b* has a constant mechanical advantage of 1.84. For $\Delta_{\text{gap}} = 0.5$, the mechanical advantage is zero, for input force less than $10N$, which means that for $F_{\text{in}} < 10N$ there is no contact between the output piston and the workpiece. For high input forces, the mechanical advantage increases until failure, which happens for $F_{\text{in}} = 90N$. For a gap of 1 mm, mechanism *b* breaks before making contact with the workpiece (see also Table 2). Mechanism *f* was designed for $\Delta_{\text{gap}} = 0.5$, and its behavior is shown in Fig. 8 with dashed lines. The mechanism has a higher mechanical advantage than mechanism *b* for $\Delta_{\text{gap}} = 0.5$ (as expected), and it requires less input force to make contact with the workpiece. However, this is achieved at the cost of lower fracture limit (maximum input force is $F_{\text{in}} = 66N$).

Next, consider optimal design of the crunching mechanism for a workpiece made of cork. The cork workpiece is assumed to fill out the gap under the output piston. It has dimensions $A = 20 \times 10(\text{mm})^2$ and $l = 20$ mm and Young's modulus $E_{\text{cork}} = 0.03GPa$. These data give the workpiece stiffness $K_s = E_{\text{cork}}A/l = 300N/\text{mm}$.

The resulting mechanism for $\Delta_{in}^{*} = 1.5$ mm is seen in Fig. 7i, and the data for the mechanism are found in Table 2. The mechanism topology resembles mechanisms designed for $\Delta_{gap} > 0$ (Figs. 7f–7h).

The prior example shows that the optimal mechanism is highly dependent on the size of the workpiece. The mechanical advantage and the fracture resistance is decreased when the workpiece does not fill the gap under the output port. *Therefore, the best mechanism performance is obtained by designing the mechanism for zero gap and using extension pieces between the workpiece and the output port to fill out a possible gap.*

The last example in this subsection shows that the input/output relation can be inverted by inverting the direction of the input force. Consider again the design example defined in Fig. 5. Now, the input force F_{in} is defined to be a force pulling away form the design domain. The input displacement is constrained to $\Delta_{in}^{*} = 1.0$ mm, the gap is zero, and all other data are the same as before. The optimal topology is seen in Fig. 9j. The figure shows that the left part of the topology corresponds to the crunching mechanism for the prior examples, and that the right part of the mechanism inverts the input force from being oriented inward to being oriented outward.

B. Compliant hand tool

To demonstrate dependence of the optimal topology on restrictions in the design domain, consider the design of a compliant hand tool shown in Fig. 10. The design goal is to maximize the mechanical advantage between the input and the output ports, subject to an input (hand) force at the handles ($F_{in} = 30N$). The tool is again made of Nylon, the thickness is $t = 10$ mm, the allowed input displacement is $\Delta_{in}^{*} = 1.0$ mm, the gap is $\Delta_{gap} = 0.01$ mm, the allowable amount of material is 50%, and the workpiece is considered stiff. The design domain is discretized by $N = 150 \cdot 50 = 7500$ elements. A similar design example is seen in Howell and Midha's work [9].

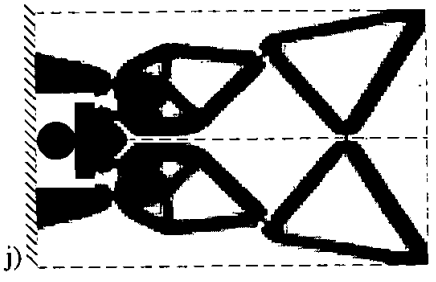

Fig. 9. Crunching mechanism for inverted input force and zero gap.

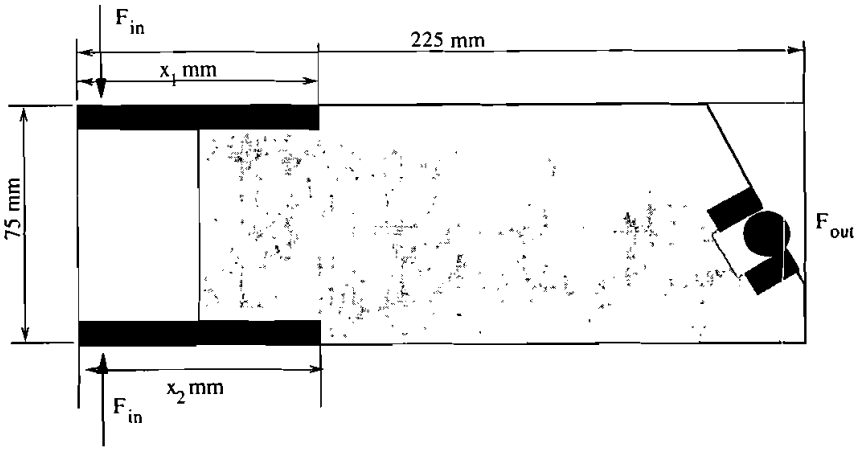

Fig. 10. Design domain for the compliant hand tool.

The design problem is solved for three different handle sizes, namely k: $x_1 = 75$ mm, $x_2 = 75$ mm, l: $x_1 = 75$ mm, $x_2 = 200$ mm, and m: $x_1 = 200$ mm, $x_2 = 160$ mm. The optimal topologies are shown in Fig. 11. The mechanical advantages and maximum stresses obtained are k: $M = 4.4$ and $\sigma_{max} = 58N/(\text{mm})^2$; l: $M = 4.8$ and $\sigma_{max} = 67N/(\text{mm})^2$, $mM = 4.5$; and $\sigma_{max} = 64N/(\text{mm})^2$, respectively.

All three solutions are seen to be four-bar mechanisms. The difference between mechanisms is the position of the hinges. As the design spaces of examples l and m are more restricted, their mechanical behavior is expected to be worse than for example k. This is not directly reflected in the value of the mechanical advantage, since the maximum stresses in the three designs are different. To make a fair comparison of the three mechanisms, the mechanical advantage to maximum stress ratio can be calculated as 0.076, 0.072, and 0.070, respectively, which shows that the less restricted mechanism k is indeed optimum among the three. It should be emphasized that this comparison of the mechanisms is heuristic, and the example shows that the introduction of direct stress constraints in the design procedure is important.

Mechanism k might be the optimum mechanism, but for manufacturing reasons, example m may be favored, since it is topologically simpler. A physical interpretation of the tool from Fig. 11m is seen in Fig. 12(top). The shapes of the narrow regions have been interpreted as half circles. However, the optimum shape of the narrow regions should be made the subject of further investigation. As suggested by Howell and Midha [9], hinges of bars that will always be under compression can be substituted with passive hinges. This is also done in the interpretation. The interpreted tool topology was cut out in Nylon (see Fig. 12(bottom)), and demonstrated the predicted behavior when tested.

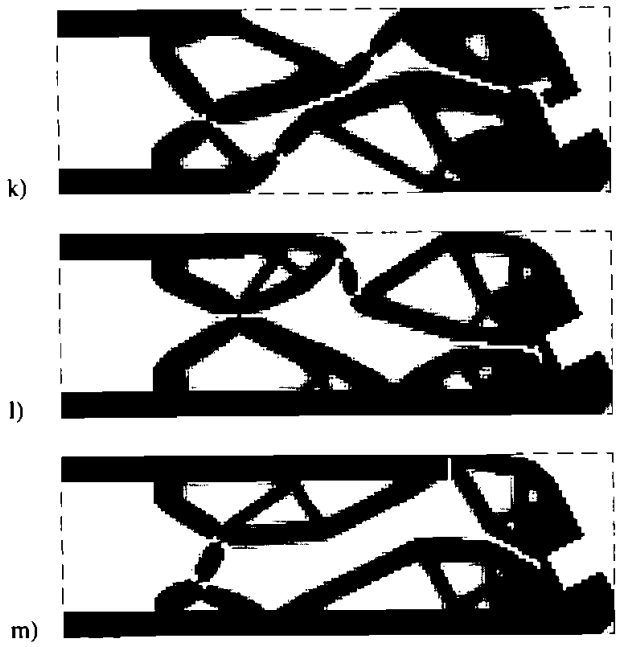

Fig. 11. The optimal hand tool topologies for different fixed handle sizes.

C. Micro gripper

A typical structure for micromanipulation purposes is a gripping device. Therefore, the design example shown in Fig. 13 (left) is considered. A horizontal input force at the mid-left side of the design domain should be converted to a closing of the jaws at the right side of the design domain. The microgripper is constructed in Silicon, which has Young's modulus $E = 180GPa = 180 \cdot 10^3 N/(\mu m)^2$ and yield strength $\sigma_f = 7GPa = 7 \cdot 10^3 N/(\mu m)^2$. For manufacturing reasons, the thickness is only $t = 7\mu m$. To allow for underetching of the structure, it must be thin; i.e, have no wide elements. This can be controlled indirectly by allowing a low volume fraction of 20%. The input force is $F_{\text{in}} = 1000\mu N$, and the workpiece (which could be a blood cell) has stiffness $K_s = 1N/\text{mm}$.

For an input displacement of $\Delta_{\text{in}}^* = 2.0\mu m$, the optimum mechanism topology is shown in Fig. 14(top left). The resulting output displacement is $\Delta_{\text{out}} = 1.3\mu m$, and the mechanical advantage is $M = 1.3$.

The output jaws of the gripping mechanism in Fig. 14(top left) open and close in a crocodile-like way, as seen in Fig. 14(bottom left) (the jaws do not move in parallel). If interest is in a gripping mechanism with parallel moving jaws, two

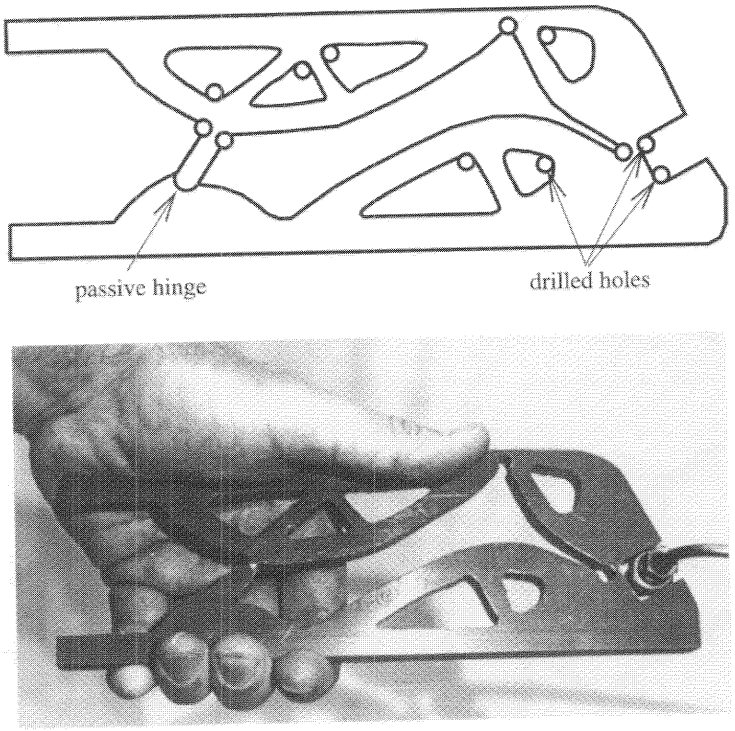

Fig. 12. Interpretation (top) and realization (bottom) of hand tool *c*.

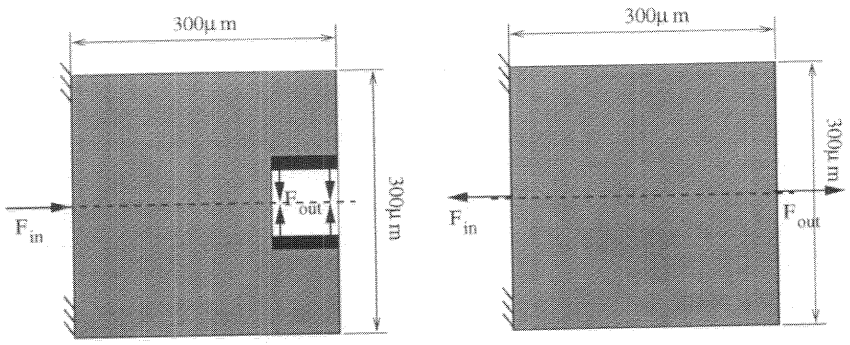

Fig. 13. Design domains for a micro gripper (left) and a micro displacement inverter and amplifier (right).

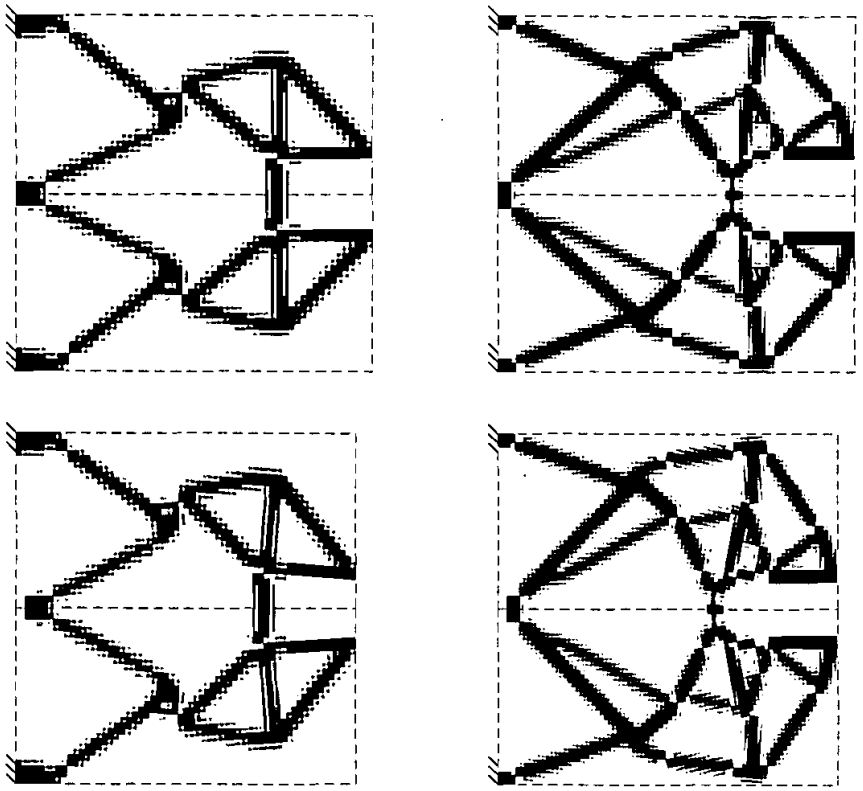

Fig. 14. Micro gripping mechanisms. Top left: optimal microgripper topology for one output port and its displacement pattern (bottom left). Top right: optimal microgripper topology for two output port and its displacement pattern (bottom right).

output ports must be considered. This is done by defining another dummy load case at the second output port (at the internal part of the jaws) and defining an extra mechanical advantage as the force relation between the extra output port and the input force. The objective function for the optimization problem in Eq. 21 then becomes

$$\Phi = -M_1 - M_2 + r(M_2 - M_1)^2 \tag{23}$$

where r is a penalty parameter. Formulating the objective function in this way, the two mechanical advantages are constrained to be equal (by least square error), and they are at the same time maximized. Furthermore, an extra displacement constraint $\Delta_{in(2)} \leq \Delta_{in}^*$ is added to the optimization problem.

Repeating the optimization problem for two output ports and workpiece stiffness $K_s = 0.5N/\mu m$, the mechanism topology in Fig. 14(top right) is obtained. From the displaced mechanism in Fig. 14(bottom right), it can be see that the output jaws now move in parallel. The two resulting mechanical advantages are $M_1 = M_2 = 0.9$ and $\Delta_{out} = 1.8\mu m$.

This example shows that a mechanism with complex output behavior can be designed by the proposed procedure.

D. Micro displacement inverter and amplifier

The optimal design of MEMS is highly dependent on the type of actuator considered. For example, a comb-drive [26], which is an electrostatic actuator, can only produce contraction forces, not expansion forces. For a specific manipulation purpose, it might, therefore, be necessary to convert the contraction force to an expansion force. Another important problem in the design of MEMS is the lack of actuators with high output displacement and, at the same time, high output force. Therefore, an important design problem in MEMS is the design of a displacement amplifier that can convert the output displacement of a large-force, small-displacement actuator (for example, a piezoelectric actuator) to a larger output displacement with minimum loss of force. The following examples demonstrate the design of a simple force inverter and a displacement amplifier and discuss the energy conversion for such mechanisms.

The dimensions are the same as for the microgripper in the previous subsection, and the design domain is sketched in Fig. 13(right). First, consider the design of a displacement (and force inverter). The input force is $F_{in} = 1000\mu N$, the workpiece stiffness is $K_s = 0.2N/\text{mm}$, and the allowed input displacement is $\Delta_{in}^* = 5.0\mu m$. The resulting mechanism is shown in Fig. 15(left). The resulting output displacement is $\Delta_{out} = 4.8\mu m$, and the mechanical advantage is $M = 0.97$. For this mechanism, the work done by the input force is calculated as $W_{in} = F_{in}\Delta_{in} = 5nJ$, and the work done by the output force is calculated as $W_{out} = F_{in}M\Delta_{out} = k_s\Delta_{out}^2 = 4.7nJ$, which means that 7% of the input work was stored as elastic energy in the mechanism. Note that if this had been a rigid-body mechanism, there would have been no "loss" of work between the input and the output ports.

Constraining the input displacement to be $\Delta_{in}^* = 2.0\mu m$ and letting the stiffness of the workpiece be $K_s = 0.03N/\text{mm}$, the resulting output displacement is $\Delta_{out} = 7.8\mu m$, and the mechanical advantage is $M = 0.23$. The mechanism can be said to be a $1 : -3.9$ displacement amplifier. The optimal topology for the mechanism is shown in Fig. 15(right). For this mechanism, the input and output works can be found to be $W_{in} = 2.0nJ$ and $W_{out} = 1.8nJ$, respectively, which means that 10% of the work was stored as elastic energy in the mechanism. If a high value of displacement amplification is needed, one could mount several of

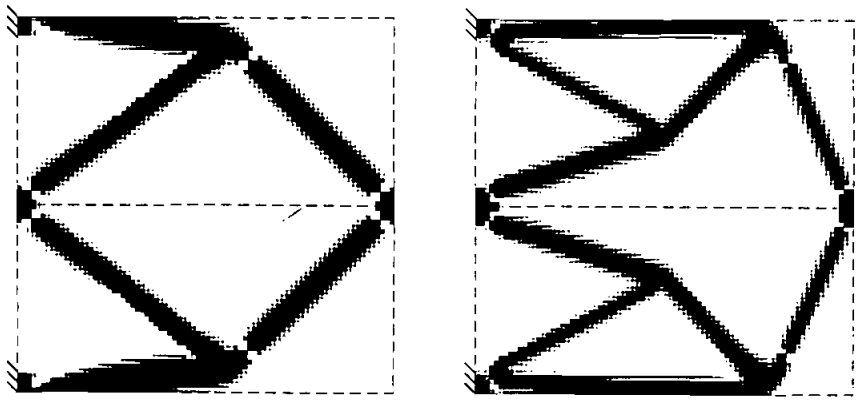

Fig. 15. Micro displacement inverters.

the 1 : −3.9 displacement amplifiers in series. However, this will result in poor work transmission, since 10% of the input work is lost for each amplifier.

The assumption of linear displacements is close to being violated for the last two design examples. If the displacement amplifier in Fig. 15(right) is studied, it is clear that the output displacement is limited by the point at which the two bars that lead to the output port become vertical. A linear displacement finite element model would not predict this locking. It is therefore clear that non-linear displacement theory must be considered, in order to generalize the design method to the design of large displacement mechanisms. This will be the subject of future research.

VI. MANUFACTURING USING LASERMICROMACHINING

Together with other devices, the two displacement inverters from subsection 5.D have been manufactured in microscale at Mikroelektronik Centret (MIC) at the Technical University of Denmark. The optimal topologies are converted into an input file for direct laser writing of a silicon layer. The resulting patterns are transferred to a PECVD-glass, which in turn is underetched to release the structures. For more details on the manufacturing processes, the reader is referred to Larsen, Sigmund, and Bouwstra's work [14].

Pictures of the processed devices are shown in Fig. 16. A handle was added to allow for testing the mechanisms. The microchip with the micromechanisms was placed on an x-y stage, and a probe was used to pull the handles. The displacement of the micromechanisms were monitored on a screen, while the handles were being pulled. Test data for the two micro displacement inverters are shown in Fig. 17. The actual displacements could be measured with an accuracy of $\pm 1 \mu m$ (resolution of the screen). From the figure, it is seen that the output displacement increases

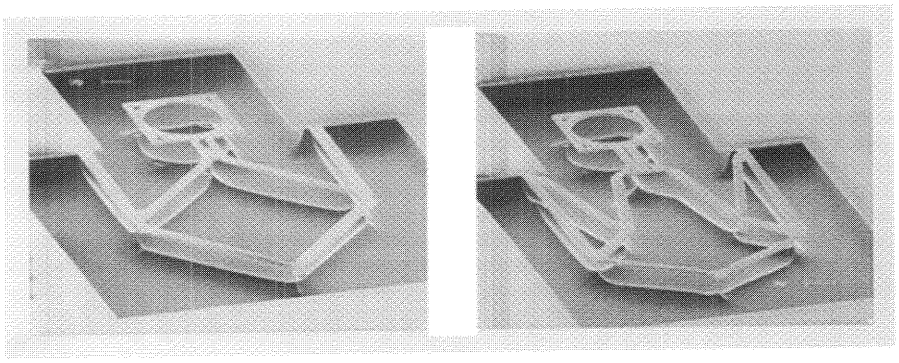

Fig. 16. Micromachined micro displacement inverters (size of the devices: 300 μm). The devices were processed at Mikroelektronik Centret, MIC, DTU, Denmark [14].

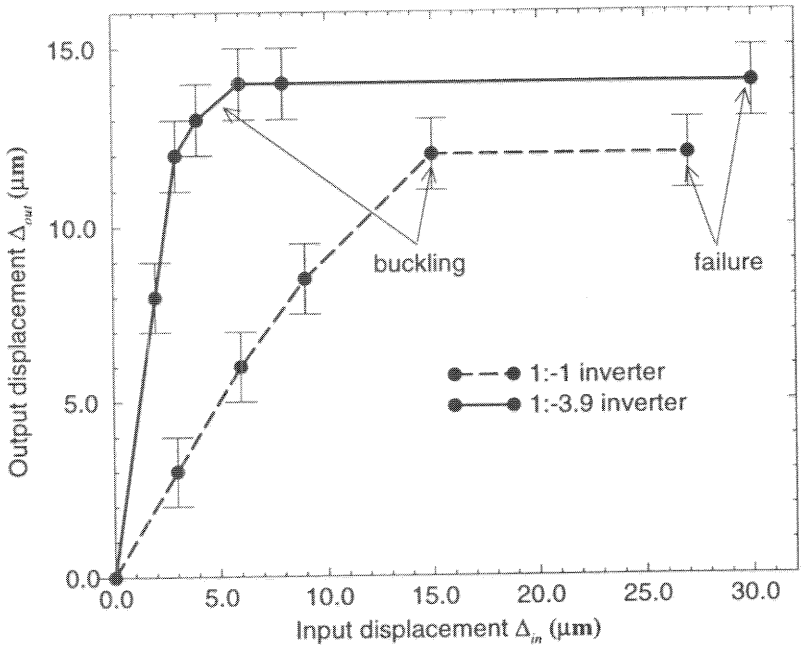

Fig. 17. Test data for micromachined devices [14].

nearly linearly, up to an output displacement of approximately $10\mu m$. Thereafter, there is no increase in the output displacement, which is explained by out of the plane buckling. Finally, for input displacements over $25\mu m$, the device breaks. The out of plane buckling phenomena could be prevented by a thicker glass layer.

Unfortunately, a glass layer thickness of more than $7\mu m$ was not possible with the available fabrication method. Apart from using a fabrication method that allows for thicker device layers, the buckling problem could also be reduced by introducing more supports for the mechanism.

VII. CONCLUSIONS

The examples presented show that the proposed method for optimal design of compliant mechanisms indeed can be used as an efficient tool for compliant mechanism synthesis. Although the method could be used as a design tool as is, much work still must be done to fully understand and optimize the behavior of compliant mechanisms.

The first extension needed is to implement direct stress constraints in the formulation. This extension will slow computational speed, but it will also result in different and improved optimum mechanism topologies. Other important extensions are the detailed modeling of flexural hinges, extensions to large displacements, and variable supports.

Ignoring stress constraints, the present method's ability to predict mechanism topologies and locate optimum positions of hinges can probably be used as an alternative method for optimal synthesis of rigid body mechanisms.

A further extension of the mechanism design procedure is to allow for two (or more) materials. If two materials have different properties—for example, two different thermal expansion coefficients—or one is passive and the other is active (piezoelectric, shape memory alloy, etc.), it will be possible to design devices that can be activated using, for example, heat or electric fields. A three-phase (two materials and void) topology optimization method for the design of material structures with extreme (also negative) thermal expansion coefficients has been suggested by Sigmund and Torquato [27,18]. This work can be used as a basis for the design of active compliant mechanisms that are composed of multiple materials.

VIII. ACKNOWLEDGEMENTS

The work presented in this paper received support from Denmark's Technical Research Council (Programme of Research on Computer-Aided Design). The author also gratefully acknowledges the work of Ulrik Darling Larsen and Siebe Bouwstra at Mikroelektronik Centret (MIC), Technical University of Denmark, who produced and tested the micromachined devices. Last but not least, the author expresses his gratitude to Martin P. Bendsœ, Pierre Duysinx, John M. Hansen, and Pauli Pedersen at Denmark's Technical University for helpful discussions and inspiration.

REFERENCES

1. N.M. Sevak and C. W. McIarnan, Optimal synthesis of flexible link mechanisms with large static deflection. *ASME Paper No. 74-Det-83*, 1974.
2. I. Her and A. Midha, A compliance number concept for compliant mechanisms and type synthesis. *Journal of Mechanisms, Transmissions and Automation in Design, Transactions of the ASME* **109**(3): 348–355 (1987).
3. R. H. Burns and F. R. E. Crossley, Kinetostatic synthesis of flexible link mechanisms, *ASME-Paper No. 68-Mech-36* 1968.
4. K. E. Petersen, Silicon as a mechanical material, *Proc. IEEE* **70**(5): 420–457 (1982).
5. C.-J. Kim, A. P. Pisano, and R. S. Muller, Silicon-processed overhanging microgripper, *Journal of Microelectromechanical Systems* **1**(1): 31–36 (1992).
6. I. Her, A. Midha, and B. A. Salamon, A methodology for compliant mechanisms design: Part II—shooting method and application. In *ASME, Advances in design automation* **44**(2): 39–45 (1992).
7. A. Midha, I. Her, and B. A. Salamon, A methodology for compliant mechanisms design: Part I—introduction and large-deflection analysis. In *ASME, Advances in design automation* **44**(2): 29–38 (1992).
8. L. L. Howell and A. Midha, A generalized loop-closure theory for the analysis and synthesis of compliant mechanisms. In *ASME Machine Elements and Machine Dynamics* **116**: 491–500 (1994).
9. L. L. Howell and A. Midha, A method for design of compliant mechanisms with small length flexural pivots, *Transactions of the ASME* **116**: 280–290 (1994).
10. M. P. Bendsœand N. Kikuchi, Generating optimal topologies in optimal design using a homogenization method, *Computational Methods in Applied Mechanics and Engineering* **71**: 197–224 (1988).
11. M. P. Bendsœ, *Optimization of Structural Topology, Shape and Material*, Springer, 1995.
12. G. K. Ananthasuresh, S. Kota, and Y. Gianchandani, A methodical approach to the design of compliant micromechanisms. In *Solid-state sensor and actuator workshop*, 189–192, 1994.
13. O. Sigmund, Some inverse problems in topology design of materials and mechanisms. In D. Bestle and W. Schielen, (ed), *Symposium on optimization of mechanical systems*, 277–284, Kluwer, Netherlands, 1996.
14. U. D. Larsen, O. Sigmund, and S. Bouwstra, Design and fabrication of compliant mechanisms and material structures with negative Poisson's ratio, *Journal of Microelectromechanical Systems*, in press.
15. B. A. Salamon and A. Midha, An introduction to mechanical advantage in compliant mechanisms. *ASME Advances in design automation* **44**(2): 47–51 (1992).
16. P. Pedersen, On the minimum mass layout of trusses. In *AGARD Conference Proceedings No. 36, Symposium on Structural Optimization*, 189–192, 1970.
17. K. Schittkowski, Numerical comparison of non-linear programming algorithms for structural optimization, *Structural Optimization* **7**(1–2): 1–19 (1994).
18. O. Sigmund and S. Torquato, Design of materials with extreme thermal expansion using a three-phase topology optimization method, *Journal of the Mechanics and Physics of Solids*, in press.
19. R. J. Hanson and K. L. Hiebert, A sparse linear programming subprogram, Technical Report SAND81-0297, Sandia National Laboratories, 1981.
20. C. S. Jog and R. B. Haber, Stability of finite element models for distributed-parameter optimization and topology design, *Computer Methods in Applied Mechanics and Engineering* **130**(3–4): 203–226 (1996).
21. A. R. Díaz and O. Sigmund, Checkerboard patterns in layout optimization, *Structural Optimization* **10**: 40–45 (1995).

22. R. B. Haber, C. Jog, and M. P. Bendsœ, A new approach to variable-topology shape optimization using a constraint on perimeter, *Structural Optimization* **11**: 1–12 (1996).
23. J. Petersson and O. Sigmund, Slope constrained topology optimization, DCAMM-report no. 538, Danish Center for Applied Mathematics and Mechanics, Lyngby, Denmark, 1977.
24. M. G. Mullender, R. Huiskes, and H. Weihnans, A physiological approach to the simulation of bone remodelling as a self-organizational controll process, *Journal of Biomechanics* **11**: 1389–1394 (1994).
25. O. Sigmund, Design of material structures using topology optimization, PhD thesis, Department of Solid Mechanics, Technical University of Denmark, 1994.
26. W. C. Tang, T.-C. H. Nguyen, M. W. Judy, and R. T. Howe, Electrostatic comb-drive of lateral polysilicon resonators. In *Transducers '89, 5th International Conference on Solid-State Sensors and Actuators*, Montreux, Switzerland, 1989.
27. O. Sigmund and S. Torquato, Composites with extremal thermal expansion coefficients, *Applied Physics Letters* **69**(21): 3203–3205, 1996.
28. W. K. Pratt, *Digital Image Processing*, Johan Wiley and Sons, New York, 1991.

Received April 1997

A. Sensitivity analysis

Solving the linear programming problem of Eq. 22 requires determination of sensitivities. The sensitivity of the mechanical advantage defined in Eq. 18 is

$$\frac{\partial M}{\partial x^e} = \frac{p_2}{p_1} \frac{(\Delta_{22} + p_2/K_s)\frac{\partial \Delta_{21}}{\partial x^e} - \frac{\partial \Delta_{22}}{\partial x^e}(\Delta_{21} - \Delta_{\text{gap}})}{(\Delta_{22} + p_2/K_s)^2} \tag{24}$$

The sensitivity of the input displacement defined in Eq. 8 is

$$\frac{\partial \Delta_{\text{in}}}{\partial x^e} = \frac{\partial \Delta_{11}}{\partial x^e} - \frac{\partial c}{\partial x^e}\Delta_{12} - c\frac{\partial \Delta_{12}}{\partial x^e} \tag{25}$$

where c is defined in Eq. 16 and the sensitivity of c is

$$\frac{\partial c}{\partial x^e} = \frac{\Delta_{22}\left(\frac{\partial \Delta_{21}}{\partial x^e} - \frac{\partial M}{\partial x^e}p_1/K_s\right) - \frac{\partial \Delta_{22}}{\partial x^e}(\Delta_{21} - Mp_1/K_s - \Delta_{\text{gap}})}{\Delta_{22}^2} \tag{26}$$

where $R = Mp_1$ was used. The sensitivity of the displacement of Eq. 2 is

$$\frac{\partial \Delta_{ij}}{\partial x^e} = -(\mathbf{d}_j^e)^T \frac{\partial \mathbf{s}^e}{\partial x^e}\mathbf{d}_i^e/p_i \tag{27}$$

where $\mathbf{s}^e$ is the 8×8 stiffness matrix of element e and $\mathbf{d}_i^e$ is an 8-vector with the nodal displacements associated with element e. Note that there is no summation over index i, on the right hand side of Eq. 27.

Defining $\mathbf{s}^0$ as the 8×8 element stiffness matrix for *solid* material, the local element stiffness matrix $\mathbf{s}^e$ for element e can be written as (using Eq. 19)

$$\mathbf{s}^e = (x^e)^{\eta}\mathbf{s}^0 \tag{28}$$

and the sensitivity of $\mathbf{s}^e$ with respect to design variable x^e can be found as

$$\frac{\partial \mathbf{s}^e}{\partial x^e} = \eta(x^e)^{\eta-1}\mathbf{s}^0 \tag{29}$$

Now, sensitivity of the displacements of Eq. 27 can be rewritten as

$$\frac{\partial \Delta_{ij}}{\partial x^e} = -\eta(x^e)^{\eta-1}(\mathbf{d}_j^e)^T\mathbf{s}^0\mathbf{d}_i^e/p_i \tag{30}$$

B. Mesh-independency algorithm

As the mesh-independency method used [25] is not available in the public literature, it is briefly described here. It must be emphasized that the method is purely heuristic, but results obtained using the method are very close to those found in theoretically well founded work [23].

The basic idea of the filter is to use blurring techniques borrowed from image processing [28]. A possible way of using image processing filters is to take a blurring filter and post-process the topology with it after each iteration. However, better performance has been achieved by use of the method described here. Most image processing filters modify the color (density) of each pixel (element), based on the colors (densities) of the immediate (4 or 9) neighbours. To ensure mesh-independency in the present problem, the filter has a fixed geometrical size, meaning that the modification of an element is dependent on elements that lie within a radius r_{min} of the considered element.

The convolution operator is written as

$$\hat{H}^f = r_{\text{min}} - \text{dist}(e, f), \{e \in N \mid \text{dist}(f, e) \leq r_{\text{min}}\}, e = 1, \ldots, N \tag{31}$$

where the operator $\text{dist}(f, e)$ is defined as the distance between the center of element e and the center of element f and. The convolution operator $\hat{H}^f$ is zero outside the filter area. The filter factor $\hat{H}^f$ for element f is seen to decay linearly with the distance from element e.

The filter itself works by modifying element relative strain energies (element sensitivities)

$$\left(\widehat{\frac{\partial \Delta_{ij}}{\partial x^e}}\right) = -\eta(x^e)^{-1}\frac{1}{\sum_{f=1}^{N}\hat{H}^f}\sum_{f=1}^{N}\hat{H}^f(x^f)^{\eta}(\mathbf{d}_j^e)^T\mathbf{s}^0\mathbf{d}_i^e/p_i \tag{32}$$

This means that instead of using the real sensitivities of Eq. 30, the filtered sensitivities of Eq. 32 are used. It is worthwhile noting that the sensitivity of Eq. 32 converges to the original sensitivity of Eq. 30 as r_{min} approaches zero.

Basically, *the filter produces a length scale r_{min}, underneath which structural variation is not allowed.* The inverse of r_{min} can therefore be interpreted as a low pass filter value that prevents rapid variations in the densities. Typically an optimization problem solution is initiated with r_{min} equal to 10% of the smaller dimension of the design domain.